European Journal of Mechanics / B Fluids 115 (2026) 204384

Contents lists available at ScienceDirect

European Journal of Mechanics / B Fluids

journal homepage: www.elsevier.com/locate/ejmflu

Heat transfer from a partially buried circular cylinder in oscillatory flow

H. Thomas [a],*, R. Stuhlmeier [c,a], A.G.L. Borthwick [a], S. Michele [b,a]

[a] University of Plymouth, School of Engineering, Computing and Mathematics, Drake Circus, Plymouth, PL4 8AA, Devon, United Kingdom
[b] University of Rome Tor Vergata, Department of Civil Engineering and Computer Science, Via del Politecnico 1, Rome, 00133, Italy
[c] Technion – Israel Institute of Technology, Faculty of Civil & Environmental Engineering, Haifa, 3200003, Israel

ARTICLE INFO

Keywords:
Boundary layers
Heat transfer
Steady streaming

ABSTRACT

With the growing abundance of man-made cylindrical structures located on or close to the seabed, it is important to be able to assess their potential environmental impact. Herein, a model is presented of the viscous-thermal boundary layer in the vicinity of a circular cylinder resting on, or partially buried in, an otherwise flat seabed. To model the influence of wave-induced motions near such a cylinder, we assume oscillatory flow in which the water particle displacements are small with respect to the cylinder radius. A perturbation expansion is utilised to derive solutions of the boundary layer equations, leading to analytical solutions at multiple orders. The unsteady temperature field for various burial depths is then determined numerically using a Crank–Nicolson scheme, and quantitative results, such as the Nusselt number at the cylinder surface, are deduced. Both diffusion and steady convection are responsible for the unsteady transport of temperature. The dynamics of the convective field enhance overall heat transfer from the cylinder and lead to the temperature being transported radially outward near to the seabed.

1. Introduction

Many examples exist of submerged circular cylinders immediately above or partially buried in the seabed which are subjected to an oscillatory flow field driven by tides and waves. These include marine oil and gas pipelines [1], mooring cables for floating offshore structures [2], and electrical cables transferring energy from a marine renewable energy device to the grid [3]. As the offshore renewable energy sector continues to expand, there is growing interest in the behaviour of marine electrical cables connecting offshore wind turbine installations to the mainland. Such cables are laid upon the seabed [4] and typically located in intermediate water depths. In transferring electrical power through these cables, energy is lost as heat which dissipates into the surrounding environment, causing potential ecosystem consequences for marine life [5].

The topic of a circular cylinder in oscillating flow has attracted the attention of many researchers using analytical (e.g., Wang [6]), numerical (e.g., An et al. [7]) and experimental (e.g., Sarpkaya [8]) techniques. Inspired by the hydrodynamic analysis of a body undergoing forced oscillation in a fluid by Stokes [9], Keulegan and Carpenter [10] identified a key dimensionless parameter ($U_0 T/D$, where U_0 is the amplitude of the speed of oscillation, T is the period of oscillation, and D is a characteristic dimension of the body). Now known as the Keulegan–Carpenter number, KC, this parameter characterises the different flow regimes experienced by a cylinder in oscillatory flow. Keulegan and Carpenter found that flow past an oscillating circular cylinder does not separate at small KC. However, Keulegan and Carpenter only considered four cases, with KC = 4 being the smallest value considered; this provided an impetus for further research.

Subsequent studies by Sarpkaya [11] and Bearman et al. [12] provided experimental confirmation of the results obtained by Keulegan and Carpenter for forces acting on a body and corresponding values of the drag coefficient. Concurrently, Honji [13] experimentally obtained high quality visualisations which indicated that the flow past a circular body is two-dimensional for KC < 2. Later, Tatsuno and Bearman [14] found that no vortex shedding occurs within this KC regime. While the aforementioned works are concerned with cylinders in open flow, no comparable studies exist of cylinders partially buried in a flat boundary. For the cases we shall consider herein, small KC number will be assumed, as will an attached and two-dimensional flow.

The dimensionless KC number is of great use in coastal engineering applications involving oscillatory flow. A pertinent practical example relates to the laying of electrical cables or pipelines on an erodible seabed, where oscillatory flow leads to the self-burial of these marine structures. In such cases, the flow field and the forces acting upon the cable or pipe will vary depending on the burial depth, and so it is necessary for designers to account for this effect. Notably, Sumer et al. [15] considered scour and self-burial of pipelines, and observed that the

* Corresponding author.
E-mail address: henry.thomas@plymouth.ac.uk (H. Thomas).

https://doi.org/10.1016/j.euromechflu.2025.204384
Received 23 May 2025; Received in revised form 6 August 2025; Accepted 1 October 2025
Available online 9 October 2025
0997-7546/

self-burial depth is a function of KC. For example, at very large values of KC $\sim \mathcal{O}(100)$, a pipeline may become entirely self-buried.

Recently, Michele et al. [16] formulated a theoretical model of the thermal boundary layer adjacent to the seabed under propagating free-surface waves. Michele et al. [17] then extended their model to include the effect of wave reflection and considered different configurations of locations and lengths of heat sources. For a flat, impermeable seabed, they found that second-order, steady convective terms play an important role in heat transport.

Using similar techniques, Richardson [18] and Davidson [19] analytically explored the thermal boundary layer around a circular cylinder immersed in oscillating flow in an open domain. Both authors conducted their analysis assuming small KC number, an approach that will be used in Section 3. However, Richardson focused solely on asymptotic limits of the Prandtl number, Pr, as Pr$\rightarrow 0, \infty$, and did not determine the solution throughout the entire domain. Later, Davidson provided more detailed insight into this problem and extended the theory to include a range of Prandtl numbers. Although both Richardson and Davidson sought steady state solutions, Michele et al. [16,17] derived an unsteady solution which furnished valuable insight into the transient phase of the heat transfer.

To the best of the authors' knowledge, heat transfer from a partially buried circular cylinder in the seabed has not been studied to date. The structure of the surrounding inviscid flow field has previously been elucidated in a series of contributions beginning with Jeffreys [20], who formulated the complex potential for a cylinder resting on a flat seabed and calculated the thrust forces on the cylinder in a steady stream. It was not until the work of Milne-Thomson [21] that the complex potential for a general burial depth was provided. Wybrow and Riley [22] successfully used this result in a study of sediment transport in oscillating flow. Wybrow & Riley determined the magnitude of the steady streaming effect and predicted the occurrence of net streaming away from the cylinder over many oscillation periods. Whereas Wybrow & Riley's theoretical analysis assumed KC $\ll 1$, their experiments were performed at KC = 0.35, complicating the comparison between theory and experiment.

The inherent difference between an open domain case and the scenario considered herein is the presence of the plane boundary. This causes a fundamental shift in the behaviour of the flow around the cylinder, which must be accounted for when considering cylindrical pipes on the seabed. Although there have been recent studies of heat transfer in the vicinity of various body geometries [23,24] in open domains, the resulting flow fields are symmetric with respect to the horizontal axis, and cannot be directly applied to a case where a boundary exists.

This paper presents a theory for heat transfer in the boundary layer close to a cylinder buried in the seabed in oscillatory flow, for a range of cases from the cylinder just touching the bed to the cylinder being partially buried. The theory presented here could potentially also be applied to offshore structures at the seabed, where progressive free-surface waves give rise to oscillatory fluid motion. The paper is structured as follows. Section 2 outlines the governing thermo-fluid equations based on conservation laws. Section 3 describes the use of a perturbation expansion technique to derive analytical first and second order solutions of the viscous boundary-layer equations, assuming small values of Keulegan–Carpenter number, KC. The end of Section 3 outlines the derivation of an important integral equality regarding the total heat exchange. Section 4 presents results for different levels of cylinder burial, obtained by numerically solving the thermal boundary-layer equation. Section 5 discusses the main findings.

2. Governing equations

The governing equations are based on mass and momentum conservation laws, along with an energy conservation equation. In the momentum equation, force components acting on the fluid are due to gravity, the pressure gradient, and viscosity. Since temperature variations are $\sim \mathcal{O}(10)$ ^{o}C, changes in fluid viscosity and density may be considered negligible [25]. Therefore, buoyancy effects are disregarded in this analysis. As found in many textbooks, e.g. White [26], for two-dimensional incompressible flow, the mass and momentum equations may be written in polar coordinates (r, θ) (see Fig. 1a) as

$$\frac{\partial (r u_r)}{\partial r} + \frac{\partial u_\theta}{\partial \theta} = 0, \tag{1}$$

$$\frac{\partial u_r}{\partial t} + u_r \frac{\partial u_r}{\partial r} + \frac{1}{r} u_\theta \frac{\partial u_r}{\partial \theta} - \frac{1}{r} u_\theta^2 = -\frac{1}{\rho}\frac{\partial P}{\partial r} + \nu \left(\frac{\partial^2 u_r}{\partial r^2} + \frac{1}{r}\frac{\partial u_r}{\partial r} + \frac{1}{r^2}\frac{\partial^2 u_r}{\partial \theta^2} - \frac{1}{r^2} u_r - \frac{2}{r^2}\frac{\partial u_\theta}{\partial \theta} \right) + g_r, \tag{2}$$

$$\frac{\partial u_\theta}{\partial t} + u_r \frac{\partial u_\theta}{\partial r} + \frac{1}{r} u_\theta \frac{\partial u_\theta}{\partial \theta} - \frac{u_r u_\theta}{r} = -\frac{1}{\rho}\frac{\partial P}{\partial \theta} + \nu \left(\frac{\partial^2 u_\theta}{\partial r^2} + \frac{1}{r}\frac{\partial u_\theta}{\partial r} + \frac{1}{r^2}\frac{\partial^2 u_\theta}{\partial \theta^2} - \frac{1}{r^2} u_\theta + \frac{2}{r^2}\frac{\partial u_r}{\partial \theta} \right) + g_\theta, \tag{3}$$

where g_r and g_θ are radial and tangential components of the acceleration due to gravity. ρ is the fluid density and ν is the kinematic fluid viscosity, both taken to be constant assuming small variation in temperature. However, the temperature T depends on the flow field via the radial and angular velocity components, (u_r, u_θ). The convective–diffusive equation for heat transport may be written [26],

$$\frac{\partial T}{\partial t} + u_r \frac{\partial T}{\partial r} + \frac{1}{r} u_\theta \frac{\partial T}{\partial \theta} = \chi \left(\frac{1}{r}\frac{\partial T}{\partial r} + \frac{\partial^2 T}{\partial r^2} + \frac{1}{r^2}\frac{\partial^2 T}{\partial \theta^2} \right), \tag{4}$$

where χ is the thermal diffusivity which is likewise taken to be constant assuming small variation in T.

When considering the thermal energy in a system, the presence of a temperature gradient may induce density variations that lead to free convection. A prescribed non-zero outer flow condition implies that the Richardson number (Ri) should be examined to determine the importance of buoyancy within the model. The flow regime depends on the non-dimensional Richardson number as follows: for Ri > 10, forced convection may be neglected; whereas for Ri $\ll 1$, free convection may be neglected [27]. The Richardson number is defined as Ri $= g\beta \Delta_T a / u_\infty^2$, where β, the coefficient of thermal expansion, is determined from experimental data [28]. From the data available for β within the temperature range examined herein, β is of the order of 10^{-4} ^{o}C^{-1}. By using the scales outlined in Section 2.2, it is seen that indeed Ri $\ll 1$, which justifies the neglect of buoyancy in the present study.

2.1. Inviscid flow about a circular cylinder buried in the seabed

The effects of viscosity are confined to a thin boundary layer in the vicinity of the body. Outside this region, the fluid may be considered inviscid and irrotational. A full description of the fluid flow past the body can be obtained by matching the solution in the outer domain with the corresponding equations at the edge of the boundary layer. This procedure will be undertaken below.

In the outer domain, we assume two-dimensional, attached fluid flow about a cylinder embedded in a horizontal plane representing the rigid, impermeable seabed. Applying potential theory in the complex plane, we derive expressions for the velocity potential and stream function. Given a fixed circular body, we require there to be no normal velocity component at its surface. For the circular body buried in the plane, the velocity at the solid boundary is therefore a function of θ only. Under the assumption that protrusion of the cylinder has negligible effect on the flow induced by water waves, flow past the cylinder and seabed can then be treated as if the cylinder were placed in a half domain of uniform flow. Given a uniform, horizontal flow of velocity magnitude u_∞ at large distance from the body, the boundary velocity U_0 (given by Milne-Thompson [21, Sec. 6.51]) is expressed,

$$U_0(\theta) = \frac{4u_\infty}{n^2} \sin^2\left(\frac{n\pi}{2}\right) \left(\sin\left(\theta + \frac{\pi}{2}(n-1)\right) + \cos\left(\frac{n\pi}{2}\right) \right)^{-1} \times$$

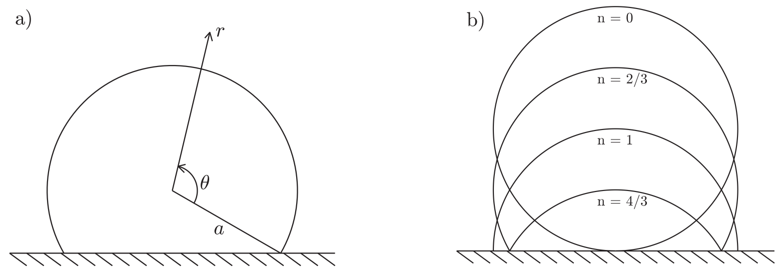

Fig. 1. *(a)* The coordinate system (r, θ) has origin at the centre of the cylinder of radius a. *(b)* Relationship between the parameter n and the burial of the cylinder.

$$\left\{ \cosh\left[\frac{2}{n} \operatorname{arccosh}\left(\cos(\tfrac{n\pi}{2}) + \frac{\sin^2\left(\frac{n\pi}{2}\right)}{\sin\left(\theta + \frac{\pi}{2}(n-1)\right) + \cos\left(\frac{n\pi}{2}\right)} \right) \right] + 1 \right\}^{-1}, \tag{5}$$

and is valid in the region

$$0 \le \theta \le \pi - 2\arcsin\left(-\cos(\tfrac{n\pi}{2})\right). \tag{6}$$

Here, the parameter $n \in [0, 2]$ determines the burial of the circular cylinder, with $n = 0$ corresponding to a circle resting on the seabed and $n = 2$ corresponding to a circle entirely buried beneath the seabed, i.e., a flat bed. Fig. 1b illustrates several typical cases for different n, where the circumferential length of the exposed pipe, L_n, can be shown to be,

$$L_n = a\pi(2 - n), \tag{7}$$

where a is the radius of the circle. Equation (5) forms the basis of the oscillatory flow field of frequency ω in the outer region, which is specified by

$$U(\theta, t) = \Re\{U_0(\theta)e^{-i\omega t}\}, \tag{8}$$

where $\Re$ denotes the real part of the expression. The direction of oscillation is parallel to the horizontal axis. As shown later, this oscillatory flow drives heat transfer, and so (8) plays an important role in this process.

2.2. Dimensionless equations for the viscous boundary layer

To obtain the viscous boundary layer equations we introduce an appropriate scaling into (1)–(3) and infer the dominant terms. To this end, these equations are written in terms of non-dimensional variables as

$$r'_{\mathrm{v}} = \frac{r - a}{\delta}, \quad \theta' = \theta, \quad u'_r = \frac{u_r}{a^{-1}\delta u_\infty}, \quad u'_\theta = \frac{u_\theta}{u_\infty}, \quad t' = \omega t, \quad P' = \frac{P}{\rho g \delta}, \tag{9}$$

where r is the radial distance from the origin, $a \sim \mathcal{O}(1)$ m is the radius of the cylinder, θ is the angle measured anticlockwise from $\theta = 0$ corresponding to the seabed, $u_\infty \sim \mathcal{O}\left(10^{-1}\right)$ m s^{-1} is the magnitude of the oscillatory outer flow velocity, t is time, $\omega \sim \mathcal{O}(1)$ rad s^{-1} is the angular frequency of the oscillatory motion at the seabed, P is pressure, $\rho = 10^3$ kg m^{-3} is taken as the approximate density of sea–water, and $g = 9.81$ m s^{-2} is acceleration due to gravity. The viscous boundary layer thickness is defined as $\delta = \sqrt{2\nu/\omega} \sim \mathcal{O}\left(10^{-3}\right)$ m [29], in which the kinematic viscosity is $\nu \approx 10^{-6}$ m^2 s^{-1}. The non-dimensionalisation procedure reveals an important parameter, known as the Keulegan–Carpenter (KC) number. This parameter $\mathrm{KC} = u_\infty/(\omega a)$ is the ratio of a characteristic flow velocity u_∞ and the product of the oscillation frequency ω with a typical length scale a. Parameters associated with the oscillatory outer flow (ω, u_∞) are chosen to align with the typical wave induced motion in water of intermediate depth compared to the wavelength [30]. With these choices we find $\mathrm{KC} \ll 1$. Here the primes denote non-dimensionalised variables.

Note that both velocity components are scaled by u_∞, the far-field velocity of the outer flow. Neglecting terms of order $\mathcal{O}(\mathrm{KC}^2)$, or higher, the mass continuity and momentum equations reduce to

$$\frac{\partial u'_r}{\partial r'_{\mathrm{v}}} + \frac{\partial u'_\theta}{\partial \theta'} = 0, \tag{10}$$

$$-g\frac{\partial P'}{\partial r'_{\mathrm{v}}} + g_r = 0, \tag{11}$$

$$\frac{\partial u'_\theta}{\partial t'} + \mathrm{KC}\left(u'_r \frac{\partial u'_\theta}{\partial r'_{\mathrm{v}}} + u'_\theta \frac{\partial u'_\theta}{\partial \theta'} \right) = \frac{g}{\omega u_\infty}\left(-\frac{\delta}{a}\frac{\partial P'}{\partial \theta'} + \frac{g_\theta}{g} \right) + \frac{1}{2}\frac{\partial^2 u'_\theta}{\partial {r'_{\mathrm{v}}}^2}. \tag{12}$$

From the radial momentum equation (11), it can be shown that the dimensional pressure term is $P = \rho g_r (r - a) + P_d(\theta)$, where the dynamic pressure P_d is independent of r. The radial variation in hydrostatic pressure in the boundary layer is $\mathcal{O}\left(\delta^2\right)$ m [29] and so can be neglected. Hence, the total pressure in the boundary layer must be the same as that exerted by the inviscid flow at the boundary. For inviscid flow, the Euler equations can be used to find an expression for P' using the outer flow solution (8). The normal velocity component is zero at the boundary, and so the angular component of the Euler equation at the boundary is

$$\frac{\partial U'}{\partial t'} + \mathrm{KC}U'\frac{\partial U'}{\partial \theta'} = \frac{g}{\omega u_\infty}\left(-\frac{\delta}{a}\frac{\partial P'}{\partial \theta'} + \frac{g_\theta}{g} \right), \tag{13}$$

with $U' = \Re\{U_0(\theta)e^{-it'}\}/u_\infty$. Substituting (13) into Eq. (12), gives the following non-dimensional boundary-layer equation

$$\frac{\partial u'_\theta}{\partial t'} + \mathrm{KC}\left(u'_r \frac{\partial u'_\theta}{\partial r'_{\mathrm{v}}} + u'_\theta \frac{\partial u'_\theta}{\partial \theta'} \right) = \frac{\partial U'}{\partial t'} + \mathrm{KC}U'\frac{\partial U'}{\partial \theta'} + \frac{1}{2}\frac{\partial^2 u'_\theta}{\partial {r'_{\mathrm{v}}}^2}. \tag{14}$$

At the solid boundary, a condition for u'_θ suffices because the solution for u'_r can be obtained by integrating (10) from 0 to r'_{v}. We impose a no-slip condition at the surface of the circular cylinder. At large radial distance, the flow is matched to that in the outer domain, i.e.,

$$u'_\theta = 0 \quad \text{on } r'_{\mathrm{v}} = 0, \tag{15}$$

$$u'_\theta = U' \quad \text{for } r'_{\mathrm{v}} \gg 1. \tag{16}$$

2.3. Dimensionless equation for the thermal boundary layer

In addition to the dimensionless, scaled equations for the viscous boundary layer, we must also employ a cognate non-dimensionalisation to obtain an equation for the thermal boundary layer from the energy equation (4). This equation is non-dimensionalised via the same scaling as (9), with the exception of the radial co-ordinate which is scaled by the thermal boundary layer thickness δ_T and distinctively denoted r'_{T}. Subsequent calculations are further simplified by non-dimensionalising and normalising T through

$$T' = \frac{T - T_{\mathrm{fluid}}}{\Delta_{\mathrm{T}}}, \tag{17}$$

where $\Delta_{\mathrm{T}} = T_{\mathrm{cyl}} - T_{\mathrm{fluid}}$ is the difference between the cylinder temperature T_{cyl} and the fluid temperature T_{fluid}. Nondimensionalising (4) it is found that both convective terms appear at order KC, whereas the radial diffusion term appears at $\mathcal{O}\left(\mathrm{KC}^2\right)$, assuming $\delta_T \sim \mathrm{KC}^{-1}\sqrt{\chi/\omega}$,

$$\frac{\partial T'}{\partial t'} + \mathrm{KC}\left(\frac{\delta}{\delta_T}u'_r\frac{\partial T'}{\partial r'_\mathrm{T}} + u'_\theta\frac{\partial T'}{\partial \theta'}\right) = \frac{\chi}{\omega\delta_T^2}\frac{\partial^2 T'}{\partial {r'_\mathrm{T}}^2} + \mathcal{O}\left(\frac{\delta_T^2}{a^2}\right). \tag{18}$$

For small KC, a perturbation expansion approach shall be used to find weakly non-linear solutions to the governing equations.

3. Perturbation expansion

3.1. First and second order solutions of the viscous boundary layer

The dimensionless Eqs. (10) and (14) for the viscous boundary layer are nonlinear and therefore not amenable to analytic treatment. The KC number appearing therein controls the contributions of the nonlinear terms. For the physical configurations considered in this study, it has been established in Section 2.2 that KC ≪ 1. We therefore progress by taking a perturbation expansion in KC, as defined in (19)–(20) below. This method enables analytical solutions for the velocity terms to be found at each order, starting from the first-order problem. In the present case it is only necessary to calculate terms up to second order in the expansion used to describe heat transfer in the boundary layer because these are the dominant terms which remain after time-averaging. The results are presented in Section 3.3 and the derivation is available in previous literature [16,19].

To this end, we write

$$u'_r = u'_{r_1} + \mathrm{KC}u'_{r_2} + \mathcal{O}(\mathrm{KC}^2), \tag{19}$$

$$u'_\theta = u'_{\theta_1} + \mathrm{KC}u'_{\theta_2} + \mathcal{O}(\mathrm{KC}^2), \tag{20}$$

where the subscripts denote ascending order terms. Substituting (19)–(20) into (10) and (14) yields the linear, leading-order system

$$\frac{\partial u'_{r_1}}{\partial r'_\mathrm{v}} + \frac{\partial u'_{\theta_1}}{\partial \theta'} = 0, \tag{21}$$

$$\frac{\partial u'_{\theta_1}}{\partial t'} - \frac{1}{2}\frac{\partial^2 u'_{\theta_1}}{\partial {r'_\mathrm{v}}^2} = \frac{\partial U'}{\partial t'}. \tag{22}$$

The boundary conditions for u'_{θ_1} are no-slip at the cylinder and match the outer inviscid flow at large distance normal to the cylinder such that

$$u'_{\theta_1} = 0 \ \text{ on } r'_\mathrm{v} = 0, \tag{23}$$

$$u'_{\theta_1} = U' \ \text{ for } r'_\mathrm{v} \gg 1. \tag{24}$$

In dimensional form, the leading order solutions are:

$$u_{\theta_1} = \Re\left\{U_0\left(1 - \mathrm{e}^{-(1-\mathrm{i})(r-a)/\delta}\right)\mathrm{e}^{-\mathrm{i}\omega t}\right\}, \tag{25}$$

$$u_{r_1} = \Re\left\{\frac{\delta}{a}\frac{\partial U_0}{\partial \theta}\left[\frac{1+\mathrm{i}}{2}(1 - \mathrm{e}^{-(1-\mathrm{i})(r-a)/\delta}) - \frac{r-a}{\delta}\right]\mathrm{e}^{-\mathrm{i}\omega t}\right\}, \tag{26}$$

the latter obtained from the equation of mass conservation (21).

At second order, the form of the (linear) equation of mass conservation (10) remains unchanged. However, the nonlinear terms in the momentum equation (14), give rise to inhomogeneities written in terms of the first order solution (25)–(26). Here it is obvious that products of such terms will contribute second harmonics of the form $\exp(-2i\omega t)$ as well as time-independent, zeroth-harmonic terms. In response to such forcing terms, we anticipate that the second-order solution will therefore be composed of identical harmonics, and write it as

$$u'_{\theta_2} = \overline{u}'_{\theta_2} + \Re\left\{\tilde{u}'_{\theta_2}\,\mathrm{e}^{-\mathrm{i}2\omega t}\right\}, \tag{27}$$

$$u'_{r2} = \overline{u}'_{r2} + \Re\left\{\tilde{u}'_{r2}\,\mathrm{e}^{-\mathrm{i}2\omega t}\right\}, \tag{28}$$

where the bar denotes time independence.

The faster oscillations at second-order merely add a small correction to the leading order solution as detailed by Mei [30], whereas the time-independent terms exert larger influence through promoting steady drift of the water particles. This phenomenon, known as *steady/acoustic streaming*, was discovered by Rayleigh [31] in a study of air circulation in a Kundt's tube (see Riley [32] for a recent comprehensive review). It is this effect which will be most consequential for the present study of heat transfer, by analogy with the case of mass transport investigated by Iskandarani and Liu [33].

We therefore consider the time-averaged equations at second order, whereupon the time-dependent terms in (27) and (28) disappear, leaving only second-order steady terms. The resulting time-averaged second-order equations are

$$0 = \frac{\partial \overline{u}'_{r_2}}{\partial r'_\mathrm{v}} + \frac{\partial \overline{u}'_{\theta_2}}{\partial \theta'}, \tag{29}$$

$$-\frac{1}{2}\frac{\partial^2 \overline{u}'_{\theta_2}}{\partial {r'_\mathrm{v}}^2} = \overline{U'\frac{\partial U'}{\partial \theta'} - u'_{r_1}\frac{\partial u'_{\theta_1}}{\partial r'_\mathrm{v}} - u'_{\theta_1}\frac{\partial u'_{\theta_1}}{\partial \theta'}}. \tag{30}$$

An appropriate boundary condition is required for $\overline{u}'_{\theta_2}$, whereas that for $\overline{u}'_{r_2}$ can be deduced from continuity of mass by integrating over the boundary layer. In a similar fashion to the leading order, we apply a no-slip condition on the circumference of the circular body. Having imposed a matching with the outer flow at leading order, at second order a no shear condition is applied at the edge of the boundary layer, yielding

$$\overline{u}'_{\theta_2} = 0 \ \text{ on } r'_\mathrm{v} = 0, \tag{31}$$

$$\frac{\partial \overline{u}'_{\theta_2}}{\partial r'_\mathrm{v}} = 0 \text{ for } r'_\mathrm{v} \gg 1. \tag{32}$$

Solving the second order Eqs. (29)–(30) along with boundary conditions (31)–(32), we obtain similar results to those found by Mei et al. [34] in 2 dimensions:

$$\overline{u}_{\theta_2} = -\frac{1}{\omega a}U_0\frac{\partial U_0}{\partial \theta}\mathcal{F}, \tag{33}$$

$$\overline{u}_{r_2} = -\frac{\delta}{a}\int_0^{(r-a)/\delta}\frac{\mathrm{d}}{\mathrm{d}\theta}\overline{u}_{\theta_2}\ \mathrm{d}r'_\mathrm{v}, \tag{34}$$

where

$$\mathcal{F} = -\frac{\mathrm{e}^{-r'_\mathrm{v}}}{2}\left(\cos(r'_\mathrm{v}) + 4\sin(r'_\mathrm{v})\right) + \frac{r'_\mathrm{v}\mathrm{e}^{-r'_\mathrm{v}}}{2}\left(\cos(r'_\mathrm{v}) - \sin(r'_\mathrm{v})\right) - \frac{1}{4}\mathrm{e}^{-2r'_\mathrm{v}} + \frac{3}{4}. \tag{35}$$

For the case $n = 1$, which is analogous to a circular cylinder in an open domain, our result agrees with the expression derived by Schlichting [29, Sec. XV].

3.2. Second-order steady streaming results for various burial depths

The foregoing solution (33)–(34) for the steady components of the second order velocity is difficult to interpret due to the complexity of the expressions for $\mathcal{F}$ and U_0. To aid understanding, we shall now visualise several cases. Due to the symmetry of the problem, only half the physical domain (depicted in Fig. 1a) will be considered. Moreover, we map the radial and angular coordinates to a rectangle to facilitate comparison with later results. Here, the vertical ordinate r'_v is simply the radial distance from the surface of the cylinder, whereas the horizontal ordinate θ is the angle, measured from the seabed to the apex of the cylinder. In all cases the angle $\theta = 0$ corresponds to the intersection of the cylinder and the seabed, whereas $\theta = \theta_s = \pi/2 + \arcsin\left(\cos\left(\frac{n\pi}{2}\right)\right)$ represents the apex of the cylinder. Note that this means the horizontal scales are different for each of the cases considered: $\theta \in [0, \pi]$ for $n = 0$, $\theta \in [0, 2\pi/3]$ for $n = 2/3$ and $\theta \in [0, \pi/2]$ for $n = 1$.

Fig. 2 shows the streamlines for the second-order time-independent solutions (33)–(34), with arrows indicating direction of flow and colours

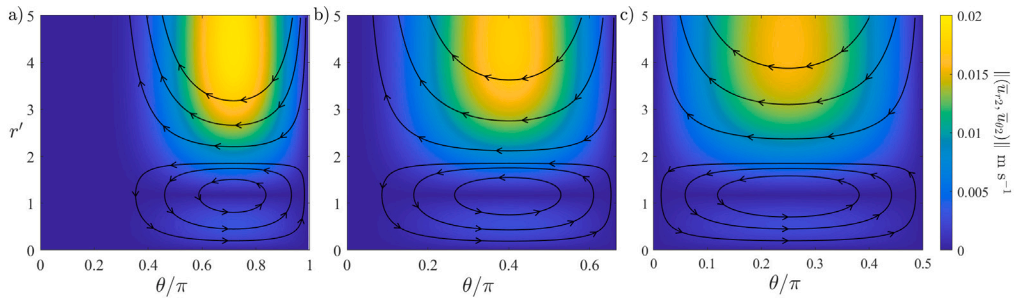

Fig. 2. Time-independent streamlines corresponding to second-order solutions of the angular and radial velocity components, $\bar{u}_{\theta_2}$ and $\bar{u}_{r_2}$, for three burial parameter cases: (a) $n = 0$; (b) $n = 2/3$; and (c) $n = 1$.

indicating flow magnitude. In each case we observe two distinct regions. Firstly, an inner boundary region with recirculating streamlines, the thickness of which is uniform for all parameters n, and is determined by the vanishing of the integral of $\mathcal{F}$, i.e.

$$\int_0^{r'_{\mathrm{v}}} \mathcal{F}\,\mathrm{d}r'_{\mathrm{v}} = 0\,, \tag{36}$$

which can be solved numerically to yield $r'_{\mathrm{v}} \approx 1.879$. In this inner boundary region, the streaming velocity is small, which limits the role of convection for $r'_{\mathrm{v}} < 1.879$. Secondly, there is an outer boundary region, $r'_{\mathrm{v}} > 1.879$, in which the streamlines are directed from the apex of the cylinder towards the seabed. As n decreases, i.e., as the cylinder protrudes to a greater extent from the seabed, there is a growing stagnation region around $\theta = 0$, seen most prominently in Fig. 2a for $n = 0$. Between the vertical lines where $\bar{u}_{r_2}$ vanishes and the border of the stagnation region, the radial velocity component is outward-pointing. This region of outward radial velocity is associated with a jet-like flow. Taking the case $n = 0$ as an example, the streamlines are directed radially outwards between the end of the stagnation region, $\theta = 0.2\pi$, and $\theta = 0.72\pi$, with the greatest magnitude of streaming occurring at $\theta = 0.52\pi$. (Note that the foregoing values were computed numerically). We therefore take $0.2\pi \le \theta \le 0.72\pi$ as the region of the jet-like flow for this case. The magnitude of the jet-like flow increases with radial distance from the cylinder, and makes a significant contribution to the convective heat transfer, as will be shown in Section 4.1. Note that Fig. 2c corresponds to the streamlines shown in physical coordinates by Schlichting and Gersten [29, Sec. XV, Figure 15.7].

Note that the effect of the boundary layer at the flat seabed can be neglected in cases when $n < 1$ because its relative strength is very small compared to that of the boundary layer around the cylinder. Moreover, the contact angle between cylinder and bed is acute and hence the net streaming is directed along the seabed. Although experiments performed by Wybrow and Riley [22] have investigated other cases, their study did not include flow visualisation, which would be of particular interest in cases where $n > 1$.

3.3. Thermal boundary layer in oscillatory flow

Following the method established by Michele et al. [17], the temperature equation (18) can be simplified considerably. This involves averaging over a fast timescale which eliminates the influence of (25)–(26), thus taking the leading order temperature to be a function of a slow timescale. Written in dimensional form, the temperature equation associated with convection from second-order streaming is

$$\frac{\partial T}{\partial t} + \bar{u}_{r_2}\frac{\partial T}{\partial r} + \bar{u}_{\theta_2}\frac{\partial T}{\partial \theta} = \chi\frac{\partial^2 T}{\partial r^2}. \tag{37}$$

Here, higher order terms in (18) have been neglected, and only the time-independent, second-order streaming velocity components play a role in convection of temperature. Even with this simplification, both $\bar{u}_{r_2}$ and $\bar{u}_{\theta_2}$ have a non-trivial dependence on (r,θ), making an analytical solution extremely challenging. To make further progress, we utilise a numerical approach.

Initially the fluid has uniform normalised temperature $T' = 0$, and the temperature of the cylinder is held constant at $T' = 1$. Exploiting the symmetry of the problem about a vertical axis through the apex of the cylinder, we impose a no flux condition at $\theta_s = \pi/2 + \arcsin\left(\cos\left(\frac{n\pi}{2}\right)\right)$. The seabed is assumed to be an adiabatic boundary, i.e. there is no heat flux at $\theta = 0$, whereas at large distances from the boundary the temperature must equal that of the outer fluid. The resulting boundary conditions are

$$T'(r,\theta,0) = 0, \tag{38}$$

$$T'(r = a,\theta,t > 0) = 1, \tag{39}$$

$$T'(r \to \infty,\theta,t) \to 0, \tag{40}$$

$$\left.\frac{\partial T'}{\partial \theta}\right|_{\theta=0,\theta_s} = 0. \tag{41}$$

In Section 4, some of our key results will be concerned with the heat flux q and total heat flux Q evaluated for each case along the circular boundary. The heat flux is described by Fourier's law,

$$q = -\kappa\left.\frac{\partial T'}{\partial r'_{\mathrm{T}}}\right|_{r'_{\mathrm{T}}=0}, \tag{42}$$

where κ is the thermal conductivity of the fluid. The total heat flux is the net flux of temperature in the domain. Due to the no-flux conditions everywhere except the boundary with the buried cylinder, we need only integrate q to give,

$$Q = 2a\int_0^{\theta_s} q\,\mathrm{d}\theta\,, \tag{43}$$

where the factor of 2 is required because the integral is evaluated in the half-domain due to symmetry.

3.4. Implicit dependence of velocity on total heat flux

It can be shown that the total heat flux Q has no explicit dependence on the convective velocity field. The necessary assumptions are made precise in the following Proposition.

Let Ω be a closed and bounded domain with an outward normal vector $\mathbf{n}$ *on the surface $\partial\Omega$, and* $\mathbf{u}$ *be a general velocity field describing an incompressible flow. Furthermore, let $\mathrm{d}V$ and $\mathrm{d}s$ represent the infinitesimals of Ω and $\partial\Omega$ respectively. If there is either no flow normal to the surface, or the temperature, T, is zero on the surface, then,*

$$\int_\Omega \nabla^2 T\,\mathrm{d}V = \frac{1}{\chi}\int_\Omega \frac{\partial T}{\partial t}\,\mathrm{d}V\,. \tag{44}$$

Expression (44) is now derived as follows. By definition,

$$Q = \oint_{\partial\Omega} \mathbf{q}\cdot\mathbf{n}\,\mathrm{d}s = \int_\Omega \nabla\cdot\mathbf{q}\,\mathrm{d}V = \int_\Omega \nabla\cdot(\nabla T)\,\mathrm{d}V = \int_\Omega \nabla^2 T\,\mathrm{d}V\,. \tag{45}$$

where the divergence theorem has been used in the second equality. Given that the fluid is incompressible (i.e., $\nabla\cdot\mathbf{u} = 0$) and that T is a finite scalar function, then,

$$T\,(\nabla \cdot \mathbf{u}) = 0\,. \tag{46}$$

We integrate the unsteady convection–diffusion equation over the region Ω to obtain,

$$\begin{aligned}\int_{\Omega} \nabla^2 T \,\mathrm{d}V &= \frac{1}{\chi}\int_{\Omega}\left[\frac{\partial T}{\partial t} + \mathbf{u}\cdot\nabla T\right]\mathrm{d}V \\ &= \frac{1}{\chi}\int_{\Omega}\left[\frac{\partial T}{\partial t} + \nabla\cdot(\mathbf{u}T)\right]\mathrm{d}V \\ &= \frac{1}{\chi}\int_{\Omega}\frac{\partial T}{\partial t}\,\mathrm{d}V + \frac{1}{\chi}\oint_{\partial\Omega}(\mathbf{u}T)\cdot\mathbf{n}\,\mathrm{d}s \end{aligned} \tag{47}$$

where we have made use of (46) and the divergence theorem. Examining the contour integral on the last line of (47), if either $T = 0$ or $\mathbf{u}\cdot\mathbf{n} = 0$ on $\partial\Omega$, the integral vanishes. Therefore we find,

$$\int_{\Omega} \nabla^2 T\,\mathrm{d}V = Q = \frac{1}{\chi}\int_{\Omega}\frac{\partial T}{\partial t}\,\mathrm{d}V\,. \tag{48}$$

In other words, the total heat flux, Q, is the volume change in temperature with time. The velocity field $\mathbf{u}$ is general and so the above result is valid for all incompressible flows, including highly turbulent flows. Moreover, the equivalency (48) can also be used to test the precision of a numerical scheme; an example is shown in Fig. 6b.

4. Numerical solution for the thermal boundary layer

The behaviour of the thermal boundary layer is determined numerically using the Crank–Nicolson scheme [35]. Eqs. (37)–(41) are spatially discretised using central differences, and the problem reduced to a linear system of equations at each time step. Due to its spatial symmetry, the physical problem is solved over the half domain $0 \le \theta \le \theta_s$.

We consider three qualitatively different scenarios, corresponding to $n = 0, 2/3$, and 1. Physically these cases represent a cylinder touching the seabed, one-quarter buried, and half buried respectively (see Fig. 1b).

To prescribe values for the dimensionless constants in our formulation, we specify a typical physical scenario. Assuming the oscillatory outer flow to be analogous to that induced by waves in water of intermediate depth, we select frequencies in the range $0.5 \le \omega \le 3$ rad s^{-1} [36]. Taking the properties of seawater using Sharqawy et al. [37] with 3% salinity at 10 °C, we use constant thermal diffusivity $\chi = 1.42\times10^{-7}\,\mathrm{m^2\,s^{-1}}$, and conductivity $\kappa = 0.587\,\mathrm{W\,m^{-1}\,{}^{\circ}C^{-1}}$ in all subsequent calculations.

Although the Crank–Nicolson scheme is unconditionally stable for a given time step, its solutions can still be subject to nonphysical oscillations, especially near a steep temperature gradient. To avoid such behaviour, the time step and grid spacing are selected to satisfy the following (grid) Péclet number (Pe) criterion (see Patankar [35]), $\mathrm{Pe} = (\Delta r, \Delta\theta)\cdot\mathbf{u}_{\max}/\chi \le 2$, for our uniform spatial discretisation Δr and $\Delta\theta$. The value of $\mathbf{u}_{\max}$ is taken to be the maximum convective velocity in each dimension, ensuring the condition is satisfied for all cases. The time step Δt satisfies the von Neumann criterion, such that $\Delta t \le \frac{1}{2}\left(\Delta r^{-2} + \Delta\theta^{-2}\right)^{-1}/\chi$. For all numerical simulations we choose $\Delta r = 8\times10^{-4}$ m, $\Delta\theta = 1.3\times10^{-3}$ rad, and $\Delta t = 1.5$ s. For further clarity on the accuracy of the scheme, grid convergence results are reported in the Appendix.

4.1. Results for various burial parameters

Although the potential theory derived by Milne-Thomson is valid for $n \in [0, 2]$, we shall consider only cases with $n \in [0, 1]$. Cases with $n > 1$ exhibit special behaviour and care must be taken in their analysis, as will be outlined in Section 4.1.4 below.

4.1.1. Case 1: $n = 0$

A cylinder touching the flat sea-bed at a single point is parameterised by $n = 0$ for $0 \le \theta \le \pi$. In this case, certain regions of the physical domain exhibit special behaviour. Near the point of contact with the seabed ($\theta = 0$) there is a region of stagnation where diffusion dominates. This can expected from an examination of the flow field in Fig. 2a, where we observe a large region of essentially zero velocity between $0 \le \theta/\pi \lesssim 0.2$. The consequence of this stagnation region is largely uniform temperature transport below $\theta/\pi \approx 0.2$, as may be seen in Fig. 3c. In this region, the temperature transport is essentially identical to the well-known solution for pure diffusion with instantaneous heating at a boundary [38, Sec. 7]:

$$T\,(r,t) = \operatorname{erfc}\left(\frac{r-a}{\sqrt{4\chi t}}\right), \tag{49}$$

where erfc is the complementary error function. For pure conduction, the heat flux normal to the cylinder can be expressed analytically as

$$q_d = -\kappa \left.\frac{\partial T}{\partial r}\right|_{r=a} = \frac{\kappa}{\sqrt{\pi\chi t}}. \tag{50}$$

At simulation times of $t_e = [100, 400, 800]$ s this yields a conductive heat flux $q_d = \kappa/\sqrt{\pi\chi t_e} = [87.9,\ 43.9,\ 31.1]\,\mathrm{W\,m^{-2}}$, whose values are used to resolve the local Nusselt number, Nu_θ, from computed heat flux; where Nu_θ is the ratio of (42) to q_d. Hence, the local Nusselt number in Figs. 3d–f remains close to unity throughout the stagnation region ($0 \le \theta/\pi \lesssim 0.2$) as expected.

Beyond the stagnation region, and up to the apex of the cylinder at $\theta = \pi$, advection plays a dominant role in the evolution of the temperature field and heat flux. After $t = 0$ s, temperature diffuses from the cylinder surface into the fluid, encountering first the inner boundary region containing the recirculating cells as seen in Fig. 2. Diffusion dominates heat transfer in this thin region (with dimensional thickness $\approx 1.879\,\delta$, recalling the result of (36)) where the velocity magnitude is small. This is apparent in Fig. 3d, where Nu_θ remains extremely close to unity throughout the domain. However, when the temperature reaches the top of the recirculating cells, the effect of outer boundary streaming becomes apparent. Streaming flow directed from the apex of the cylinder to the seabed drives the asymmetry observed in the heat flux; i.e., the heat flux can be seen to increase at the apex of the cylinder.

In the outer boundary region there is a change in the sign of the radial velocity $\bar{u}_{r_2}$, in opposition to the flow in the inner boundary region. The most striking visualisation of this is the jet in the temperature field in Fig. 3c, which becomes more apparent with increasing r'_{T} because $\mathcal{F} \to \frac{3}{4}$ as $r'_{\mathrm{T}} \to \infty$ (see (35)). Hence, for increasing r'_{T}, (33) is constant whereas (34) increases linearly.

4.1.2. Case 2: $n = 1$

The case $n = 1$ represents a circular cylinder half buried in the seabed, which is equivalent to a full cylinder in open flow, where $0 \le \theta \le \pi/2$. Unlike cases with $n < 1$, no stagnation region exists at $\theta = 0$, and the temperature field is largely determined by advection. This behaviour is explained by the streamlines depicted in Fig. 2c, where we recall that the flow in the outer boundary region is directed from the apex of the cylinder towards the seabed. The effect of this streaming is clear in Fig. 4c, where the temperature field is compressed near $\theta = \pi/2$, but the temperature increases at the seabed, $\theta = 0$.

For the case $n = 1$ there is a monotonic increase in the heat flux in the angular direction from the seabed to the apex of the cylinder. This is in accordance with the streamlines within the outer boundary layer, and confirms that the outer streaming overwhelms the flow inside the recirculating cells. The effect of Keulegan–Carpenter number on q is evident in Figs. 4d–f. With decreasing KC (i.e., increasing ω), the heat flux across the cylinder tends to a uniform value $q = q_d$. This is due to the convective terms in (18) having a coefficient directly proportional to KC. These terms disappear entirely in the limit $\mathrm{KC} \to 0$

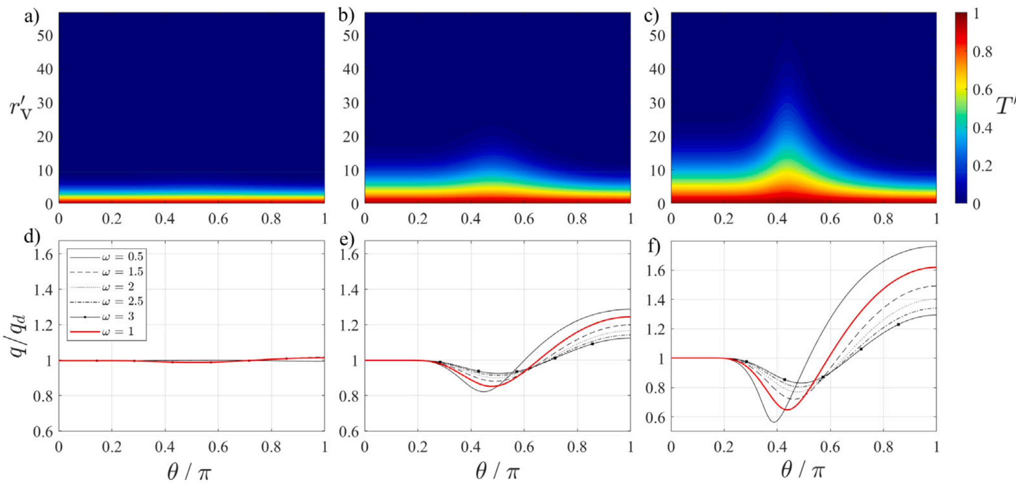

Fig. 3. Numerically predicted thermal behaviour near a circular cylinder of radius $a = 1$ m at a horizontal seabed for $n = 0$ at $t = [100, 400, 800]$ s: (a)–(c) contour plot of temperature field for $u_\infty = 0.03\,\mathrm{m\,s^{-1}}$ and $\omega = 1\,\mathrm{rad\,s^{-1}}$; and (d)–(f) Nu_θ at $r'_T = 0$ for $u_\infty = 0.03\,\mathrm{m\,s^{-1}}$ and $\omega = (0.5, 1, 1.5, 2, 2.5, 3)\,\mathrm{rad\,s^{-1}}$.

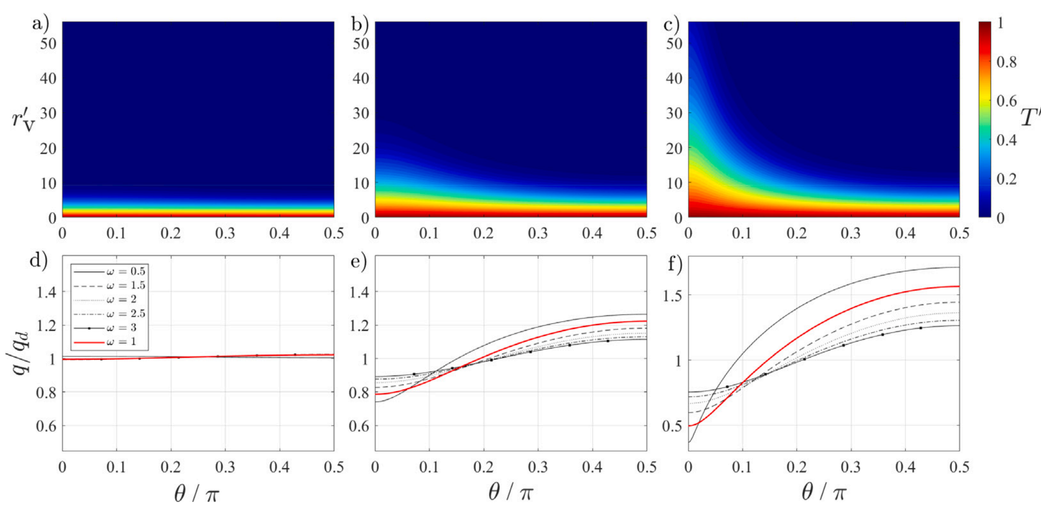

Fig. 4. Numerically predicted thermal behaviour near a circular cylinder of radius $a = 1$ m at a horizontal seabed for $n = 1$ at $t = [100, 400, 800]$ s: (a)–(c) contour plot of temperature field for $u_\infty = 0.03\,\mathrm{m\,s^{-1}}$ and $\omega = 1\,\mathrm{rad\,s^{-1}}$; and (d)–(f) Nu_θ at $r'_T = 0$ for $u_\infty = 0.03\,\mathrm{m\,s^{-1}}$ and $\omega = (0.5, 1, 1.5, 2, 2.5, 3)\,\mathrm{rad\,s^{-1}}$.

leaving only diffusive effects. Most clearly seen in Fig. 4f are the various intersection points of the normalised heat flux curves with 1 as ω increases. The intersection point tends to $\theta = \pi/4$, which is the expected result if angular convection is neglected, since the radial streaming velocity component $\bar{u}_{r_2} = 0$ at $\theta = \pi/4$. This demonstrates the relative importance of the radial convection term compared to the angular convection term, because although both terms disappear in the limit KC $\rightarrow 0$, it is the radial streaming velocity component, $\bar{u}_{r_2}$, that has the greatest influence on heat flux.

4.1.3. Case 3: n = 2/3

The intermediate case $n = 2/3$ of a quarter-buried cylinder exhibits behaviour characteristic of both $n = 0$ and 1, and so is an interesting case to explore. The range of the angular coordinate is $0 \leq \theta \leq 2\pi/3$. Fig. 2b displays the streamlines, which show behaviour similar to that observed when $n = 0$, albeit with a smaller stagnation region near $\theta = 0$. Convection in the outer boundary region creates a jet in the temperature field, similar to that for the case $n = 0$, whose maximum is close to $\theta = 0.2\pi$, the location of the maximum of $\bar{u}_{r_2}$. It is clear to see the jet located at $0 < \theta < 0.2\pi$ in Fig. 5c is largely influenced by the streamlines, and so the transport of heat is directed radially outward from the pipe and along the seabed.

Examining the heat flux in Figs. 5d–f, the curves display the same dependence upon the KC number as the previous cases; decreasing KC reduces the magnitude of the observed heat flux to pure diffusion. In all cases where $n < 1$, the minimum value of heat flux remains approximately the same, with its location coinciding with the peak of the jet.

4.1.4. Case 4: n >1

For $n > 1$, the streaming velocity field exhibits distinct behaviour caused by the outer flow when the cylinder is more than half buried in the seabed. The intersection between the cylinder and the seabed is a stagnation point from which U_0 increases to a maximum at the apex of the cylinder. However, as n increases from 1 to 2, the gradient of the outer flow (5) at $\theta = 0$ tends towards infinity, creating unphysically large streaming velocity components localised along the seabed. This accords with the second-order streaming components defined by (33)–(34), which depend on U_0 and its derivative. The non-physical velocity magnitude is largely determined by the radial velocity component, which involves the square of the derivative.

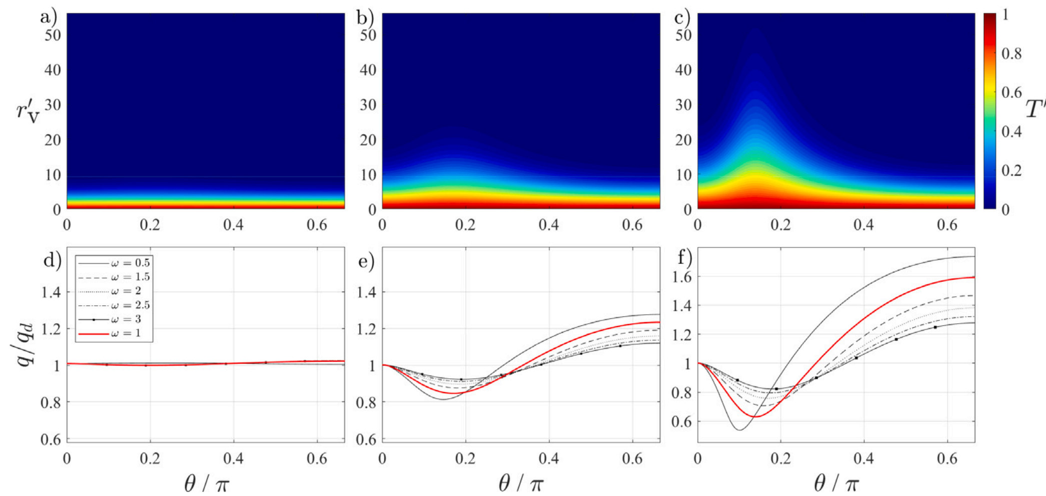

Fig. 5. Numerically predicted thermal behaviour near a circular cylinder of radius $a = 1$ m at a horizontal seabed for $n = 2/3$ at $t = [100, 400, 800]$ s: (a)–(c) contour plot of temperature field for $u_\infty = 0.03\,\mathrm{m\,s^{-1}}$ and $\omega = 1\,\mathrm{rad\,s^{-1}}$; and (d)–(f) Nu_θ at $r'_\mathrm{T} = 0$ for $u_\infty = 0.03\,\mathrm{m\,s^{-1}}$ and $\omega = (0.5, 1, 1.5, 2, 2.5, 3)\,\mathrm{rad\,s^{-1}}$.

When n becomes greater than unity, the geometry of the burial configuration changes and the contact angle between the cylinder and the seabed becomes obtuse, as shown in Fig. 1. While the theory we have developed remains formally applicable, the study by Wybrow and Riley [22] indicates that it is no longer appropriate to neglect the flow along the seabed itself. Indeed, as n is increased from 1 to 4/3, the relative magnitude of outward streaming at the stagnation point (i.e., $\theta = 0$) observed in the outer boundary region and the induced streaming along the flat seabed itself (obtained by a procedure analogous to that described in Section 3.2, for a flat bed) increases from approximately 0.1 to unity. Treatment of these competing boundary layers would require a different modelling approach, and the inclusion of a new scale for the angular variable which would be of the order of the viscous boundary layer. The interaction between these boundary layers may be expected to result in a net streaming whose direction differs from that obtained above.

4.2. Total heat flux

Fig. 6a shows the temporal development of the normalised total heat flux per unit exposed circumferential length of pipe at the pipe surface ($r'_\mathrm{T} = 0$) when $u_\infty = 0.03$ m s^{-1} and $\omega = 1$ rad s^{-1}. Here, the total heat flux, Q, is determined from (43) and the exposed pipe length, L_n, is given by (7). For increasing burial, as $n \to 2$, Q also decreases because there is less exposed pipe. However, as can be seen in Fig. 6a, the normalised heat flux increases as the burial increases. This agrees with the heat flux curves presented in Sections 4.1.1–4.1.3. For example, taking $\mathrm{Nu}_\theta = 1$ as the baseline, a greater portion of the heat flux curve is above 1 for $n = 1$ than for $n = 0$. This implies that the absence of a stagnation region results in an increase in total heat flux per unit exposed length of pipe. As anticipated from the temperature field contour plots, which are parameterised equivalently to Fig. 6a, Q is initially the same as the pure conductive heat flux for each value of n considered. The role of convection in enhancing heat transfer as time increases becomes evident as the curves of Q begin to diverge from q_d. In Fig. 6a the threshold at which this occurs is at $t \approx 250$ s. It is instructive to determine a general fit for the total heat flux, which can be applied to intermediate values of the burial parameter, i.e., $n \in [0, 1]$. Using MATLAB's fitting toolbox, an accurate and appropriate formula is found to be

$$Q(n,t) = \frac{L_n}{250}\,(0.6n - 1)^3\,(t - 450) + 811\,t^{-0.46} - 5.1 \tag{51}$$

with an r-square value of 0.99 and a root mean square value of 0.29.

Furthermore, Fig. 6a is also used to justify the run time of the numerical simulations. In all cases, there is an initial transient phase lasting about 500 s during which the total heat flux follows a steep downward gradient. This is followed by a slower monotonic decrease in Q, which tends to zero with increasing time. This decline is partly driven by the radial convective component directed outward from the cylinder. In the outer boundary region, $\bar{u}_{r_2}$ increases linearly with r'_V, eventually violating the perturbation assumptions. The selected simulation time of 800 s enables the dynamics of interest to be captured without violating the model assumptions.

5. Conclusions

This paper has presented a theoretical model of heat transfer in the oscillatory thermal boundary layer of a circular cylinder resting on, or partially buried within, an otherwise flat seabed. First, a second-order analytical expression for velocity in the viscous boundary layer was derived using a perturbation expansion, with the Keulegan–Carpenter number (KC) used as a small parameter. The energy equation was then solved numerically for temperature using a Crank–Nicolson scheme, and key quantities including heat flux were deduced. An important integral equality was derived pertaining to the total heat flux, which if the same boundary conditions are imposed, is general to any velocity field. This result was further used to validate the precision of the numerical scheme.

It was found that the burial depth of the circular cylinder has a significant effect on the temperature profile in the thermal boundary layer. Cases where the cylinder is more than three-quarters buried in the seabed exhibit non-physical streaming velocities near the seabed, therefore the temperature field for these was not analysed. In the special case when the cylinder is half buried, analogous to a full cylinder in open flow, the temperature is transported along the seabed. When the cylinder is more than half exposed, a jet in the temperature field emerges close to the seabed and directed away from the cylinder. Second-order time-independent streaming velocity components are responsible for this behaviour, and play a crucial role in temperature transport after many oscillation periods. On assessing the streamline pattern of the second-order streaming flow, distinct inner and outer regions were observed within the viscous boundary layer. In the outer boundary region, the streamlines were found to be directed towards the inner boundary region near the apex of the circular cylinder but radially outwards near the seabed for all cases studied. This has the

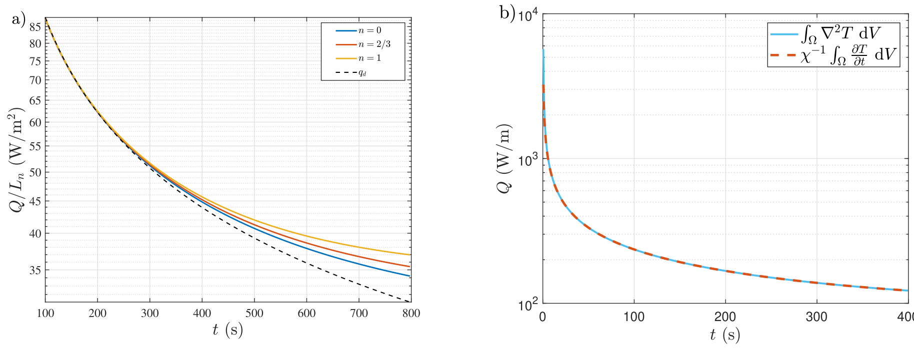

Fig. 6. Heat flux time histories for $u_\infty = 0.03$ m s^{-1} and $\omega = 1$ rad s^{-1}: (*a*) total heat flux per unit exposed circumferential length, Q/L_n, with time for three cases of burial parameter, namely $n = 0$, $2/3$, 1; and (*b*) comparative example showing the equality in (48) for $n = 1$.

effect of limiting the temperature transport into the outer domain near the apex of the cylinder.

The heat flux along the exposed boundary of the circular cylinder was calculated for various small KC values, by varying the angular frequency ω of the oscillatory outer flow. It was found that as ω increases, the KC value correspondingly decreases, with the heat flux tending to a purely diffusive state. This is a consequence of non-dimensionalisation, whereby the convective terms are scaled by KC.

We have treated the seabed as a flat, rigid and adiabatic boundary, which is an idealised simplification of the physical seabed. Theoretically, second-order steady streaming could also be used as a model for mass transport within the viscous boundary layer. If introduced into the thermal model, second-order streaming could have a distinct influence on the heat transfer, and complement the theory presented above. Conjugate heat transfer within the seabed would be dominated by conduction and may provide a satisfying addition to the model. However, to encapsulate the physical complexities of an actual seabed would require considerable computational resources, intricately coupled equations and multiple scales, which is beyond the scope of the present study.

Our current approach to heat transfer has employed the more common Eulerian approach to fluid mechanics. It may be of interest for future work to consider analytical, Lagrangian approaches to the heat-transfer problem, such as those which have recently been successfully applied to the related topic concerning free-surface boundary layers [39].

Moreover, the present model assumes that the velocity field is independent of temperature, and that density and viscosity have constant values. Further refinements of the theory, including the addition of buoyancy driven convection, and extension to turbulent flow may present fruitful avenues for future research.

CRediT authorship contribution statement

H. Thomas: Writing – original draft. **R. Stuhlmeier:** Supervision. **A.G.L. Borthwick:** Supervision. **S. Michele:** Supervision.

Funding

This work was supported by the Engineering and Physical Sciences Research Council [EP/W524554/1].

Declaration of competing interest

The authors declare that they have no known competing financial interests or personal relationships that could have appeared to influence the work reported in this paper.

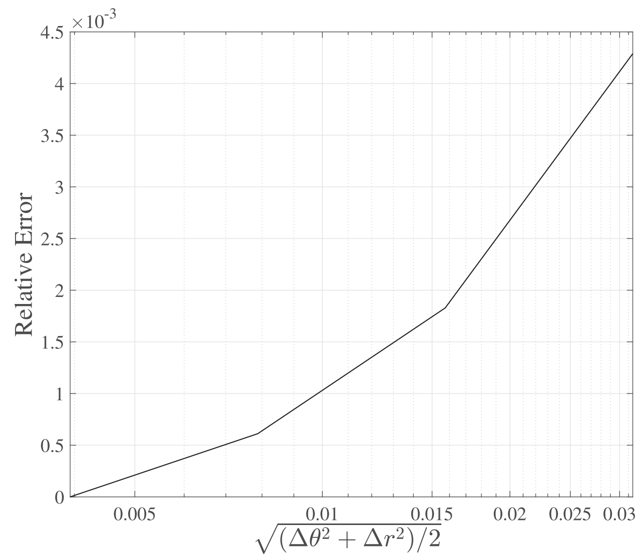

Fig. A.7. Grid convergence results.

Appendix

The results for grid convergence are reported here. The process requires a benchmark simulation on a very fine mesh, with which subsequent simulations with larger mesh sizes are compared. For the finest mesh, denoted M_{fine}, the discretisation in the spatial dimensions is chosen as $\Delta\theta = 1 \times 10^{-3}$ and $\Delta r = 2 \times 10^{-4}$. The coarser mesh sizes, denoted M_n, are related to the fine mesh via $M_n = 2^n M_{fine}$; where $n = [1, 2, 3]$ in Fig. A.7. The Relative Error is the root mean square of the difference between the temperature field on M_n and M_{fine} at time = 800 s. In all cases the cylinder is half buried i.e., $n = 1$, and $\Delta t = 1$ which satisfies the stability criteria. It is clear from Fig. A.7 that the solution converges as the mesh is refined, providing evidence for the accuracy of our simulations.

Data availability

No data was used for the research described in the article.

References

[1] M.J. Kaiser, Offshore oil and gas records circa 2020, Ships Offshore Struct. 17 (1) (2022) 205–241, http://dx.doi.org/10.1080/17445302.2020.1827633.

[2] A.C. Pillai, T.J. Gordelier, P.R. Thies, C. Dormenval, B. Wray, R. Parkinson, L. Johanning, Anchor loads for shallow water mooring of a 15 MW floating wind turbine — Part I: Chain catenary moorings for single and shared anchor scenarios, Ocean Eng. 266 (2022) http://dx.doi.org/10.1016/j.oceaneng.2022.111816.
[3] J.-A. Pérez-Rúa, K. Das, N.A. Cutululis, Optimum sizing of offshore wind farm export cables, Int. J. Electr. Power Energy Syst. 113 (2019) 982–990, http://dx.doi.org/10.1016/j.ijepes.2019.06.026, URL https://www.sciencedirect.com/science/article/pii/S014206151931018X.
[4] T. Dong, H. Brakelmann, G.J. Anders, Analysis method for the design of long submarine cables, Renew. Sustain. Energy Rev. 171 (2023) 113029, http://dx.doi.org/10.1016/j.rser.2022.113029, URL https://www.sciencedirect.com/science/article/pii/S1364032122009108.
[5] B. Taormina, J. Bald, A. Want, G. Thouzeau, M. Lejart, N. Desroy, A. Carlier, A review of potential impacts of submarine power cables on the marine environment: Knowledge gaps, recommendations and future directions, Renew. Sustain. Energy Rev. 96 (2018) 380–391, http://dx.doi.org/10.1016/j.rser.2018.07.026, URL https://www.sciencedirect.com/science/article/pii/S1364032118305355.
[6] C.-Y. Wang, On high-frequency oscillatory viscous flows, J. Fluid Mech. 32 (1) (1968) 55–68, http://dx.doi.org/10.1017/S0022112068000583.
[7] H. An, L. Cheng, M. Zhao, Steady streaming around a circular cylinder near a plane boundary due to oscillatory flow, J. Hydraul. Eng. 137 (1) (2011) 23–33, http://dx.doi.org/10.1061/(ASCE)HY.1943-7900.0000258.
[8] T. Sarpkaya, Experiments on the stability of sinusoidal flow over a circular cylinder, J. Fluid Mech. 457 (2002) 157–180, http://dx.doi.org/10.1017/S002211200200784X.
[9] G.G. Stokes, On the Effect of the Internal Friction of Fluids on the Motion of Pendulums, Trans. Camb. Philos. Soc. 9 (1851) 8–106.
[10] G.H. Keulegan, L.H. Carpenter, Forces on cylinders and plates in an oscillating fluid, J. Res. Natl. Bur. Stand. 60 (1958) 423–440, URL https://api.semanticscholar.org/CorpusID:124303029.
[11] T. Sarpkaya, Force on a circular cylinder in viscous oscillatory flow at low Keulegan2014Carpenter numbers, J. Fluid Mech. 165 (1986) 61–71, http://dx.doi.org/10.1017/S0022112086002999.
[12] P.W. Bearman, M.J. Downie, J.M.R. Graham, E.D. Obasaju, Forces on cylinders in viscous oscillatory flow at low keulegan-carpenter numbers, J. Fluid Mech. 154 (1985) 337–356, http://dx.doi.org/10.1017/S0022112085001562.
[13] H. Honji, Streaked flow around an oscillating circular cylinder, J. Fluid Mech. 107 (1981) 509–520, http://dx.doi.org/10.1017/S0022112081001894.
[14] M. Tatsuno, P.W. Bearman, A visual study of the flow around an oscillating circular cylinder at low keulegan–carpenter numbers and low Stokes numbers, J. Fluid Mech. 211 (1990) 157–182, http://dx.doi.org/10.1017/S0022112090001537.
[15] B.M. Sumer, C. Truelsen, T. Sichmann, J. Fredsøe, Onset of scour below pipelines and self-burial, Coast. Eng. 42 (4) (2001) 313–335, http://dx.doi.org/10.1016/S0378-3839(00)00066-1, URL https://www.sciencedirect.com/science/article/pii/S0378383900000661.
[16] S. Michele, R. Stuhlmeier, A.G.L. Borthwick, Heat transfer in the seabed boundary layer, J. Fluid Mech. 928 (2021) R4, http://dx.doi.org/10.1017/jfm.2021.842.
[17] S. Michele, A.G.L. Borthwick, T.S. van den Bremer, The laminar seabed thermal boundary layer forced by propagating and standing free-surface waves, J. Fluid Mech. 956 (2023) A11, http://dx.doi.org/10.1017/jfm.2023.21.
[18] P.D. Richardson, Heat transfer from a circular cylinder by acoustic streaming, J. Fluid Mech. 30 (2) (1967) 337–355, http://dx.doi.org/10.1017/S0022112067001466.
[19] B.J. Davidson, Heat transfer from a vibrating circular cylinder, Int. J. Heat Mass Transfer 16 (9) (1973) 1703–1727, http://dx.doi.org/10.1016/0017-9310(73)90163-4, URL https://www.sciencedirect.com/science/article/pii/0017931073901634.
[20] H. Jeffreys, On the transport of sediments by streams, Math. Proc. Cambridge Philos. Soc. 25 (3) (1929) 272–276, http://dx.doi.org/10.1017/S0305004100013979.
[21] L.M. Milne-Thomson, Theoretical hydrodynamics, in: Dover Books on Physics, Dover Publications, 2013, URL https://books.google.co.uk/books?id=YrTDAgAAQBAJ.
[22] M.F. Wybrow, N. Riley, Oscillatory flow over a cylinder resting on a plane boundary, European J. Appl. Math. 7 (6) (1996) 545–558, http://dx.doi.org/10.1017/S0956792500002564.
[23] Y. Zhou, G. Jiang, Y. Jiang, J. Sun, H. Li, Z. Zhou, Study on heat transfer characteristics of elliptical heat exchange tubes under acoustic streaming, Int. J. Heat Fluid Flow 112 (2025) 109738, http://dx.doi.org/10.1016/j.ijheatfluidflow.2024.109738, URL https://www.sciencedirect.com/science/article/pii/S0142727X24004636.
[24] A. Gopinath, A.F. Mills, Convective heat transfer from a sphere due to acoustic streaming, J. Heat Transf. 115 (2) (1993) 332–341, http://dx.doi.org/10.1115/1.2910684, arXiv:https://asmedigitalcollection.asme.org/heattransfer/article-pdf/115/2/332/5718124/332_1.pdf.
[25] L.D. Landau, E.M. Lifshitz, Fluid Mechanics, vol. 6, Pergamon, 2013, URL https://books.google.co.uk/books?id=CeBbAwAAQBAJ.
[26] F.M. White, Viscous Fluid Flow, McGraw-Hill, 2006, URL https://books.google.co.uk/books?id=T4cpAQAAMAAJ.
[27] F.P. Incropera, Fundamentals of Heat and Mass Transfer, Wiley, 2007.
[28] G.S. Kell, Precise representation of volume properties of water at one atmosphere, J. Chem. Eng. Data 12 (1) (1967) 66–69.
[29] H. Schlichting, K. Gersten, Boundary-layer theory, McGraw Hill, 2017, http://dx.doi.org/10.1007/978-3-662-52919-5.
[30] C.C. Mei, The Applied Dynamics of Ocean Surface Waves, World Scientific, 1989, http://dx.doi.org/10.1142/0752, arXiv:https://www.worldscientific.com/doi/pdf/10.1142/0752.
[31] J.W. Strutt, I. On the circulation of air observed in kundt's tubes, and on some allied acoustical problems, Philos. Trans. R. Soc. Lond. 175 (1884) 1–21, http://dx.doi.org/10.1098/rstl.1884.0002, arXiv:https://royalsocietypublishing.org/doi/pdf/10.1098/rstl.1884.0002.
[32] N. Riley, Steady streaming, Annu. Rev. Fluid Mech. 33 (1) (2001) 43–65, http://dx.doi.org/10.1146/annurev.fluid.33.1.43.
[33] M. Iskandarani, P.L.-F. Liu, Mass transport in two-dimensional water waves, J. Fluid Mech. 231 (1991) 395–415, http://dx.doi.org/10.1017/S0022112091003440.
[34] C.C. Mei, M. Stiassnie, D.K.-P. Yue, Theory and Applications of Ocean Surface Waves, World Scientific, 2005, http://dx.doi.org/10.1142/5566, arXiv:https://www.worldscientific.com/doi/pdf/10.1142/5566.
[35] S.V. Patankar, Numerical heat transfer and fluid flow, in: Series on Computational Methods in Mechanics and Thermal Science, Hemisphere Publishing Corporation (CRC Press, Taylor & Francis Group), 1980, URL http://www.crcpress.com/product/isbn/9780891165224.
[36] H.U. Sverdrup, M. Johnson, R. Fleming, The Oceans: Their Physics, Chemistry, and General Biology, Prentice-Hall, 1942.
[37] M.H. Sharqawy, J.H. Lienhard, S.M. Zubair, Thermophysical properties of seawater: A review of existing correlations and data, Desalination Water Treat. 16 (1–3) (2010) 354–380, http://dx.doi.org/10.5004/dwt.2010.1.
[38] C.C. Mei, Mathematical Analysis in Engineering: How to Use the Basic Tools, Cambridge University Press, 1995, pp. 132–164.
[39] S. Michele, E. Renzi, A.G.L. Borthwick, T.S. van den Bremer, Heat transfer and mass transport in the ocean wave-driven free-surface boundary layer, J. Fluid Mech. 1010 (2025) A7, http://dx.doi.org/10.1017/jfm.2025.308.